

---

**Supporting Information for**

**Morphological and optical properties of carbonaceous aerosol particles from ship emissions and biomass burning during a summer cruise measurement in the South China Sea**

**Cuizhi Sun<sup>1</sup>, Yongyun Zhang<sup>1</sup>, Baoling Liang<sup>1,&</sup>, Min Gao<sup>1</sup>, Xi Sun<sup>1,#</sup>, Fei Li<sup>1,4</sup>, Xue Ni<sup>1</sup>, Qibin Sun<sup>1</sup>, Hengjia Ou<sup>1</sup>, Dexian Chen<sup>1</sup>, Shengzhen Zhou<sup>1,2,3\*</sup>, and Jun Zhao<sup>1,2,3\*</sup>**

<sup>1</sup> School of Atmospheric Sciences, Guangdong Province Key Laboratory for Climate Change and Natural Disaster Studies, and Southern Marine Science and Engineering Guangdong Laboratory (Zhuhai), Sun Yat-sen University, Zhuhai, Guangdong 519082, China

<sup>2</sup> Guangdong Provincial Observation and Research Station for Climate Environment and Air Quality Change in the Pearl River Estuary, Zhuhai, Guangdong 519082, China

<sup>3</sup> Key Laboratory of Tropical Atmosphere-Ocean System, Ministry of Education, Zhuhai, Guangdong 519082, China

<sup>4</sup> Xiamen Key Laboratory of Straits Meteorology, Xiamen Meteorological Bureau, Xiamen, Fujian 361012, China

<sup>&</sup> Now at Guangzhou Environmental Monitoring Center, Guangzhou, Guangdong 510060, China

<sup>#</sup> Now at Centre for Isotope Research (CIO), Energy and Sustainability Research Institute Groningen (ESRIG), University of Groningen, Groningen 9747 AG, the Netherlands

*Correspondence to:* Jun Zhao ([zhaojun23@mail.sysu.edu.cn](mailto:zhaojun23@mail.sysu.edu.cn)) and Shengzhen Zhou ([zhoushz3@mail.sysu.edu.cn](mailto:zhoushz3@mail.sysu.edu.cn))

20 This supplement contains 8 sections, 1 table and 14 figures.

---

## 1. Calculation of the cut size diameter of the TEM sampler

A single-stage cascade impactor, equipped with a jet nozzle of 0.3 mm in diameter, was used for single particle sampling. The Stokes number is defined in Eqs. (1–2) (Marple and Olson, 2011). The cut-size diameter, which is defined as the diameter corresponding to a 50% collection efficiency, can be derived using Eq. (3).

$$Stk = \frac{\rho_p C_c d_p^2 U}{9\eta W} \quad (1)$$

$$U = \frac{Q}{\pi \left(\frac{W}{2}\right)^2} \quad (2)$$

$$d_{p_{50}} = \sqrt{Stk_{50}} \sqrt{\frac{9\eta\pi W^3}{4\rho_p C_c Q}} \quad (3)$$

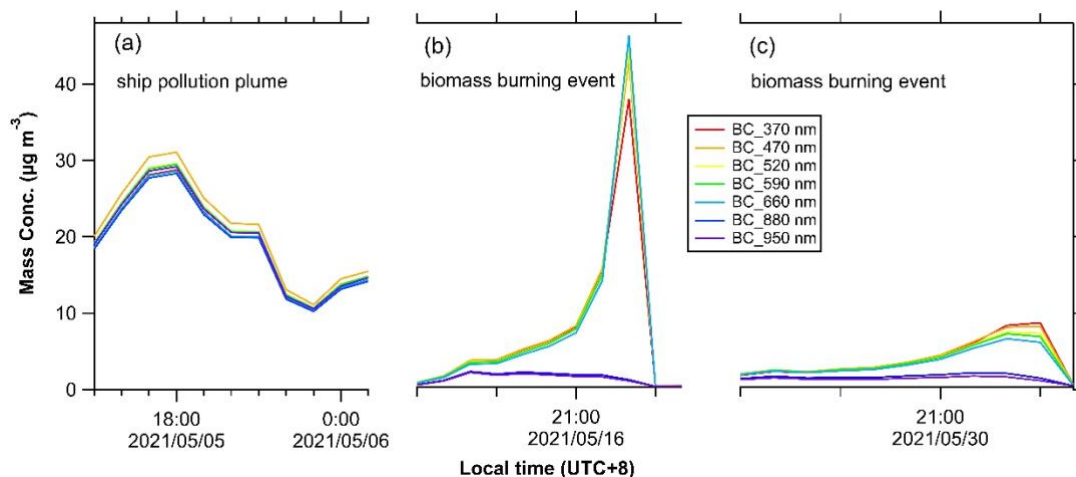
where  $Stk$  is Stokes number, and the square root of the  $Stk$  corresponding to 50% collection efficiency ( $\sqrt{Stk_{50}}$ ) is 0.47 assumed a jet Reynolds number of 3000;  $\rho_p$  is particle density assumed as 1.5 g cm<sup>-3</sup>;  $C_c$  is Cunningham's slip correction factor, approximately 1;  $\eta$  is air (or gas) viscosity, 1.8134×10<sup>-5</sup> Pa·s at 293 K, a constant under normal atmospheric condition.  $U$  represents the average air (or gas) velocity at the nozzle exit;  $Q$  is the volumetric flow rate through the nozzle and is equal to 1 L min<sup>-1</sup>;  $W$  is the nozzle diameter and is 0.3 mm;  $d_{p_{50}}$  is the cut point particle diameter at the 50% collection efficiency.

## 2. Biomass burning events and the AAE calculation

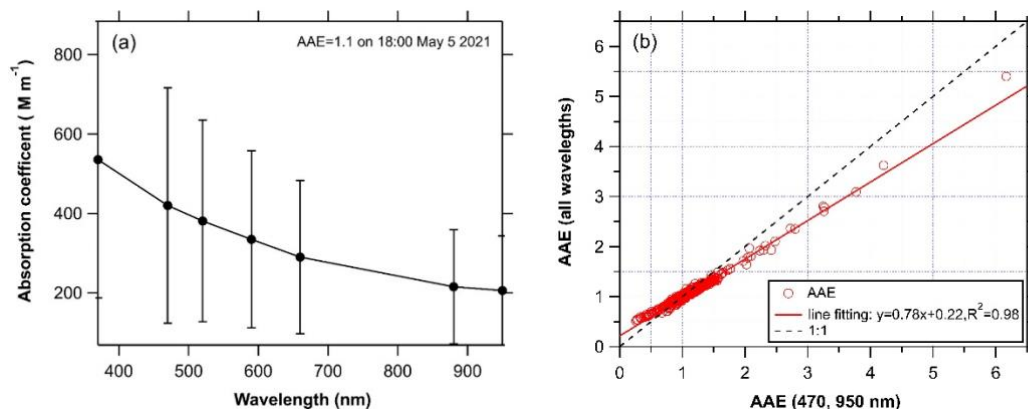
The long-range biomass burning transport affects the air mass in the South China Sea (SCS). Figure S1 illustrates an example of the wavelength-dependent mass concentration measured by the aethalometer (Model AE33, Magee Scientific, USA) during the campaign, showing (a) the own ship plume emitted from the vessel itself, and (b and c) two significant biomass burning events, both lasting for 10 hours on May 16 and 30, 2021. The ship plumes, predominantly emitted from the foil fuel burning, show similar absorption at all seven wavelengths. In contrast, significant absorption at low wavelengths was detected during the biomass burning events, a phenomenon also observed in other field measurements in urban cities/towns where air masses were susceptible to biomass burning (Zhang et al., 2017).

Two methods were used to obtain the hourly absorption Ångström exponent (AAE) values from the

AE33 measurements. Figure S2a shows an example of the AAE calculation for a ship plume at 18:00 on May 5. Figure S2b demonstrates the linear relationship between the AAE values obtained from all 50 wavelengths and those obtained from a pair of wavelengths at 470 and 950 nm. The fitting results indicate that AAE (all wavelengths) was lower than AAE (470, 950 nm) with a fitting slope of 0.78 and a determination coefficient ( $R^2$ ) of 0.98.



55 **Figure S1.** The wavelength-dependent mass concentration from the AE33 aethalometer for (a) ship pollution plume, (b, c) two significant biomass burning events during the campaign.



60 **Figure S2.** (a) A ship plume at 18:00 on May 05 for the wavelength-dependent absorption Angström exponent (AAE) based on the hourly averaged data, (b) AAE obtained from all the wavelengths vs the AAE obtained from two wavelengths at 470 and 950 nm based on hourly averaged data during the campaign.

---

### 3. Single particle analysis using the ImageJ's plugin

Figure S3 shows examples of TEM images using the software program ImageJ for single particle analysis.

65 Figure S3a is captured before beam focus, which is subsequently used for single particle analysis in  
Figure S3b. However, particles No. 2 and No. 13 (indicated by the red arrow) were manually excluded  
from the statistical analysis due to overcounting. In Figure S3c, volatile components were vaporized after  
beam focus, leaving nonvolatile composition such as BC residual on the substrate (e.g., particles  
indicated by the blue arrow). The outline of BC aggregates was extracted using ImageJ's Frac Lac plugin  
70 (deep ImageJ) for fractal dimension calculation, which is based on the boxing counting method, for  
example, the image inside the blue rectangle on the lower right corner of Figure S3c.

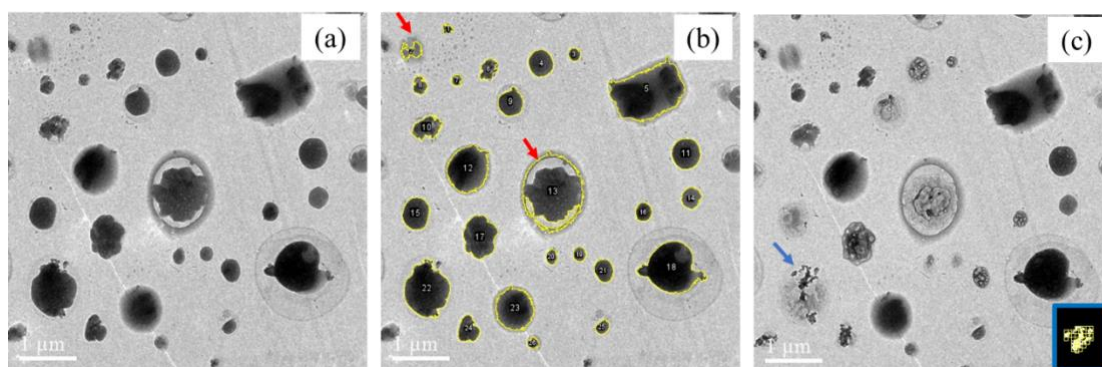
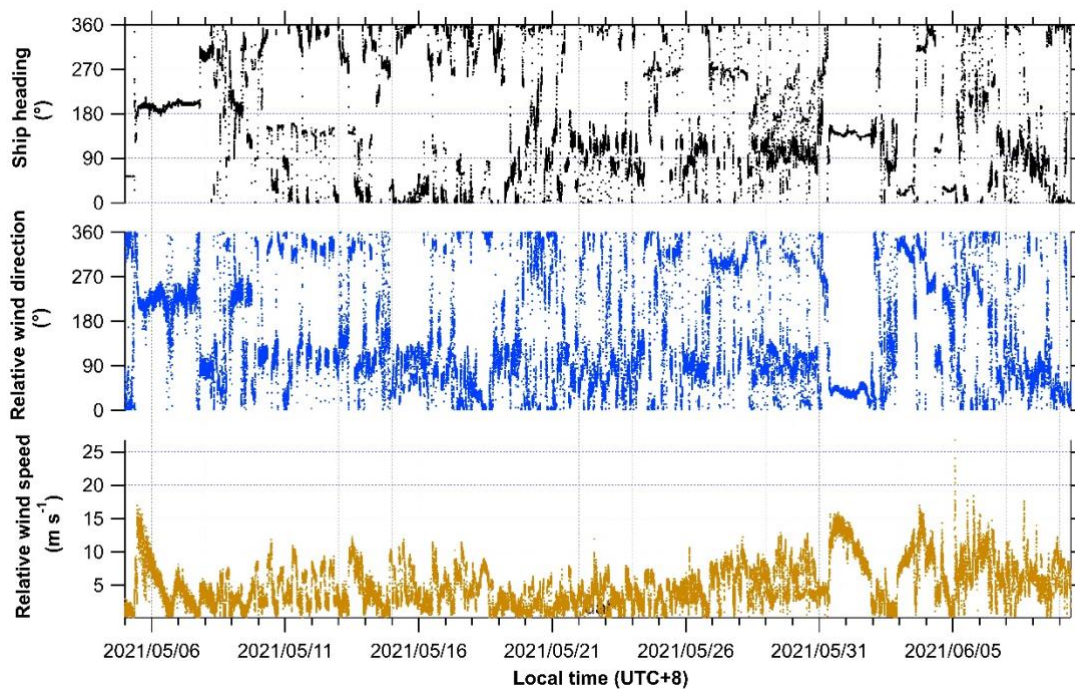


**Figure S3.** Example images of the single particle analysis using ImageJ's plugin: (a) Before beam focus  
75 in the TEM image, (b) particles marked with numbers in yellow using ImageJ, and (c) after beam focus  
in the TEM image.

### 4. Meteorological data for single particle sampling during navigation and stop

The time series of ship heading, relative wind direction (RWD), and relative wind speed (RWS) with a  
3-sec time resolution in the South China Sea during the campaign (May 05–June 09, 2021) is shown in  
80 Figure S4. The RWD and RWS varied considerably and frequently due to the operational starts and stops  
(halts) of the ship for other tasks. The 10-min averaged RWD and RWS data were determined based on  
vector calculations. Detailed meteorological data, encompassing the 10-min average for single particle  
sampling during navigation and stop, are listed in Table S1. The sampling location for single particle  
sampling is shown in Figure S5.

85 Note that the samples collected during navigation were free from interference from the own ship emission due to high relative wind speeds ( $>5 \text{ m s}^{-1}$ ) and appropriate relative wind directions ( $0^\circ\text{--}80^\circ$ ,  $280^\circ\text{--}360^\circ$ ). Samples collected with wind speeds below  $5 \text{ m s}^{-1}$  or at relative wind direction in the range of  $80^\circ\text{--}280^\circ$  were air masses mixed with the own ship emissions.



90 **Figure S4.** Time series of ship heading, relative wind direction (RWD), and relative wind speed (RWS) during the campaign in the South China Sea (SCS).

**Table S1.** Meteorological data on the 10-min average single particle sampling during navigation and stop.

| Serial number | Sampling start time | P (hPa)          | RH (%)         | S.R. ( $\text{W m}^{-2}$ ) | Temp. ( $^\circ\text{C}$ ) | RWS* ( $\text{m s}^{-1}$ ) | RWD* ( $^\circ$ ) |
|---------------|---------------------|------------------|----------------|----------------------------|----------------------------|----------------------------|-------------------|
| N1            | 2021/5/10 11:18     | $1008.3 \pm 0.0$ | $81.0 \pm 0.7$ | $961.9 \pm 42.4$           | $29.7 \pm 0.0$             | $10.5 \pm 0.6$             | $341.7 \pm 50.7$  |
| N2            | 2021/5/11 8:24      | $1007.9 \pm 0.0$ | $83.3 \pm 0.5$ | $491.6 \pm 10.1$           | $28.9 \pm 0.1$             | $9.8 \pm 0.5$              | $320.2 \pm 46.7$  |
| N3            | 2021/5/11 19:00     | $1006.6 \pm 0.1$ | $75.5 \pm 0.5$ | -                          | $29.7 \pm 0.0$             | $6.4 \pm 0.8$              | $336.1 \pm 21.1$  |
| N4            | 2021/5/12 8:13      | $1007.5 \pm 0.1$ | $78.8 \pm 0.6$ | $474.5 \pm 32.9$           | $29.4 \pm 0.1$             | $7.0 \pm 0.4$              | $327.7 \pm 53.1$  |
| N5            | 2021/5/15 19:15     | $1006.6 \pm 0.0$ | $77.8 \pm 1.9$ | -                          | $30.2 \pm 0.1$             | $6.2 \pm 0.7$              | $60.1 \pm 37.2$   |
| N6            | 2021/5/16 12:35     | $1007.5 \pm 0.0$ | $76.9 \pm 0.7$ | $989.8 \pm 13.2$           | $29.8 \pm 0.0$             | $10.8 \pm 0.7$             | $340.3 \pm 59.0$  |
| N7            | 2021/5/17 14:40     | $1006.6 \pm 0.0$ | $72.2 \pm 0.9$ | $758.7 \pm 7.7$            | $30.0 \pm 0.0$             | $10.0 \pm 0.6$             | $16.9 \pm 47.7$   |

---

|     |                 |              |            |               |            |            |              |
|-----|-----------------|--------------|------------|---------------|------------|------------|--------------|
| N8  | 2021/5/18 8:47  | 1009.3 ± 0.0 | 79.3 ± 0.5 | 647.1 ± 68.5  | 30.1 ± 0.0 | 7.3 ± 0.5  | 12.3 ± 59.7  |
| N9  | 2021/5/18 18:10 | 1007.0 ± 0.0 | 75.8 ± 0.4 | 28.5 ± 6.1    | 30.7 ± 0.0 | 5.3 ± 0.4  | 14.2 ± 50.4  |
| N10 | 2021/5/21 16:16 | 1006.2 ± 0.1 | 74.0 ± 0.5 | 244.8 ± 62.2  | 30.2 ± 0.0 | 6.0 ± 1.2  | 16.8 ± 29.5  |
| N11 | 2021/5/22 15:32 | 1005.3 ± 0.0 | 82.1 ± 0.7 | 551.3 ± 140.5 | 28.5 ± 0.1 | 6.3 ± 1.0  | 57.4 ± 19.6  |
| N12 | 2021/5/27 8:55  | 1009.2 ± 0.0 | 76.1 ± 0.7 | 666.6 ± 16.4  | 29.8 ± 0.1 | 7.0 ± 0.4  | 291.8 ± 45.9 |
| N13 | 2021/6/1 18:07  | 1004.7 ± 0.0 | 76.1 ± 0.3 | 78.6 ± 14.6   | 30.3 ± 0.0 | 8.0 ± 0.5  | 40.0 ± 45.2  |
| N14 | 2021/6/3 10:50  | 1005.4 ± 0.1 | 77.9 ± 0.7 | 151.9 ± 6.7   | 30.1 ± 0.0 | 10.1 ± 0.5 | 313.2 ± 61.3 |
| N15 | 2021/6/8 10:18  | 1008.8 ± 0.0 | 86.2 ± 0.4 | 259.7 ± 40.5  | 28.4 ± 0.1 | 5.1 ± 0.7  | 58.6 ± 19.7  |
| S1  | 2021/5/9 14:36  | 1007.2 ± 0.0 | 74.6 ± 0.5 | 739.4 ± 164.0 | 29.4 ± 0.1 | 1.8 ± 0.7  | 242.4 ± 62.3 |
| S2  | 2021/5/9 15:30  | 1006.6 ± 0.1 | 75.3 ± 0.8 | 686.9 ± 32.3  | 29.5 ± 0.2 | 3.0 ± 0.6  | 238.5 ± 42.3 |
| S3  | 2021/5/13 9:07  | 1006.6 ± 0.0 | 77.1 ± 0.6 | 709.6 ± 12.6  | 30.4 ± 0.0 | 0.1 ± 1.3  | 222.1 ± 32.9 |
| S4  | 2021/5/13 19:15 | 1005.8 ± 0.0 | 65.0 ± 1.4 | -             | 30.4 ± 0.1 | 5.5 ± 2.1  | 95.9 ± 67.1  |
| S5  | 2021/5/14 10:50 | 1006.9 ± 0.0 | 75.4 ± 0.5 | 932.7 ± 4.1   | 30.9 ± 0.1 | 2.4 ± 0.7  | 193.3 ± 38.7 |
| S6  | 2021/5/16 21:50 | 1008.3 ± 0.1 | 77.3 ± 0.8 | -             | 29.8 ± 0.1 | 3.7 ± 0.5  | 68.3 ± 48.3  |
| S7  | 2021/5/18 21:12 | 1008.0 ± 0.0 | 77.0 ± 0.0 | -             | 30.5 ± 0.0 | 0.5 ± 0.4  | 128.1 ± 51.4 |
| S8  | 2021/5/19 8:42  | 1008.2 ± 0.0 | 74.8 ± 0.6 | 661.4 ± 6.3   | 31.0 ± 0.1 | 2.1 ± 0.6  | 123.0 ± 32.5 |
| S9  | 2021/5/20 18:00 | 1007.7 ± 0.1 | 68.5 ± 0.5 | 54.4 ± 8.6    | 31.6 ± 0.1 | 0.3 ± 0.3  | 109.5 ± 40.4 |
| S10 | 2021/5/22 8:40  | 1008.0 ± 0.1 | 73.8 ± 0.6 | 278.1 ± 136.2 | 30.2 ± 0.1 | 1.3 ± 0.3  | 43.1 ± 66.1  |
| S11 | 2021/5/23 8:39  | 1007.6 ± 0.1 | 74.9 ± 0.7 | 646.7 ± 9.9   | 30.1 ± 0.1 | 3.2 ± 0.6  | 83.0 ± 61.8  |
| S12 | 2021/5/23 20:43 | 1008.6 ± 0.0 | 80.4 ± 0.7 | -             | 29.1 ± 0.1 | 3.6 ± 0.6  | 91.5 ± 69.4  |
| S13 | 2021/5/24 8:01  | 1009.3 ± 0.0 | 74.9 ± 0.3 | 526.1 ± 10.5  | 30.3 ± 0.1 | 2.5 ± 0.5  | 133.4 ± 43.6 |
| S14 | 2021/5/24 16:03 | 1007.1 ± 0.0 | 75.7 ± 0.8 | 94.5 ± 4.9    | 30.4 ± 0.1 | 2.4 ± 0.7  | 76.9 ± 48.1  |
| S15 | 2021/5/25 9:21  | 1010.1 ± 0.0 | 77.6 ± 0.5 | 734.1 ± 86.0  | 29.8 ± 0.1 | 4.7 ± 0.5  | 317.3 ± 47.0 |
| S16 | 2021/5/30 22:11 | 1002.9 ± 0.1 | 96.0 ± 0.0 | -             | 27.3 ± 0.0 | 2.0 ± 0.3  | 108.9 ± 68.7 |
| S17 | 2021/6/2 9:10   | 1007.2 ± 0.0 | 78.5 ± 0.5 | 675.9 ± 17.1  | 29.8 ± 0.1 | 3.1 ± 0.4  | 17.6 ± 42.1  |
| S18 | 2021/6/5 18:23  | 1003.0 ± 0.1 | 83.8 ± 0.4 | 2.3 ± 0.5     | 29.0 ± 0.1 | 11.8 ± 0.9 | 279.0 ± 36.0 |
| S19 | 2021/6/7 8:45   | 1006.7 ± 0.1 | 86.3 ± 0.9 | 110.9 ± 36.6  | 27.8 ± 0.1 | 4.1 ± 3.2  | 105.5 ± 45.3 |

---

95 \* The relative wind direction and wind speed are 10-min vector average.

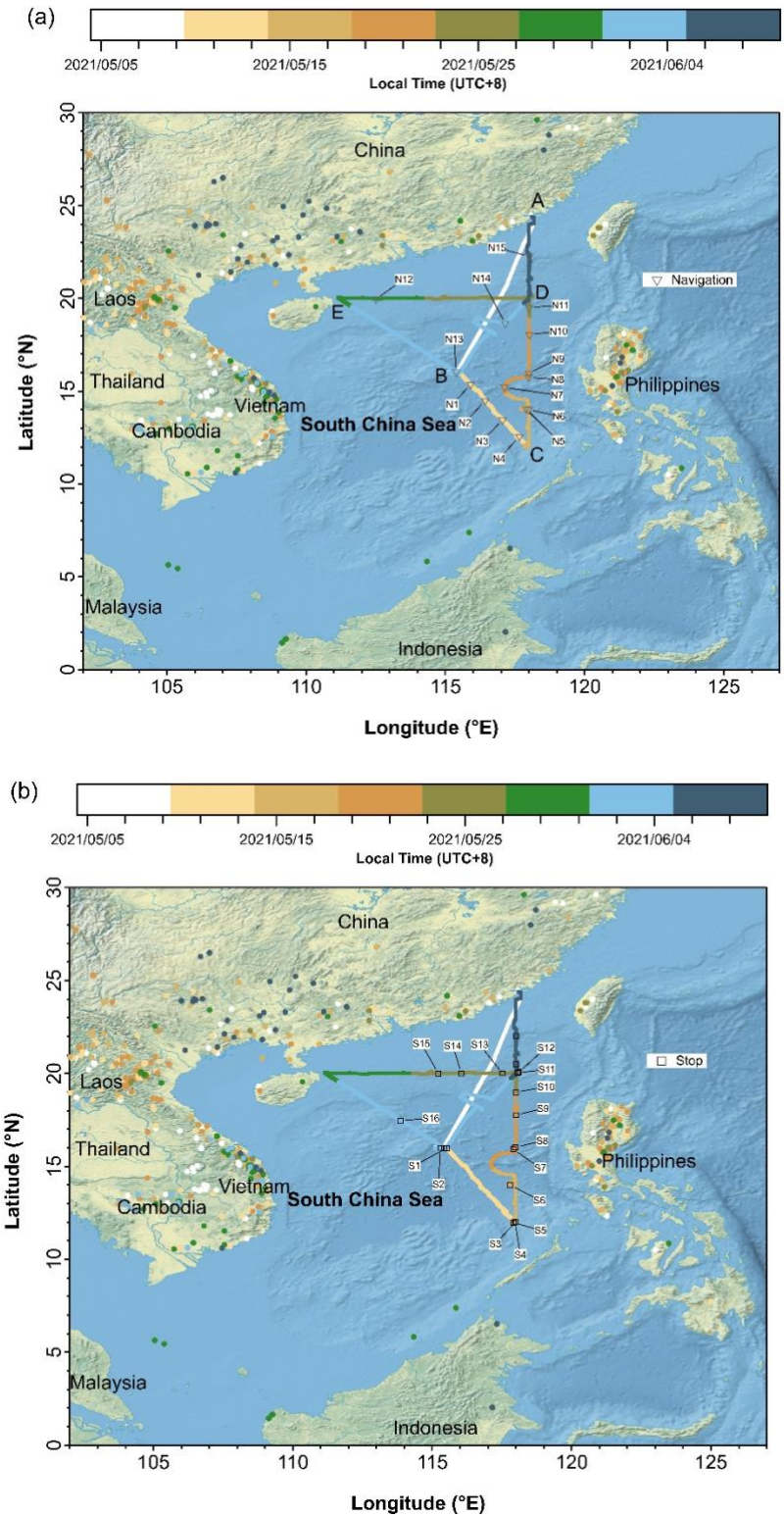


**Figure S5.** Map of the ship route in the South China Sea during the campaign. The open triangles in (a) and squares in (b) indicate the single particle sampling location, collected during navigation and stop. The samples marked in N1 to N15 for navigation sampling and S1 to S19 for stop sampling in serial. The solid circles indicate the fire spots with a confidence level greater than 80% using MODIS satellite data.

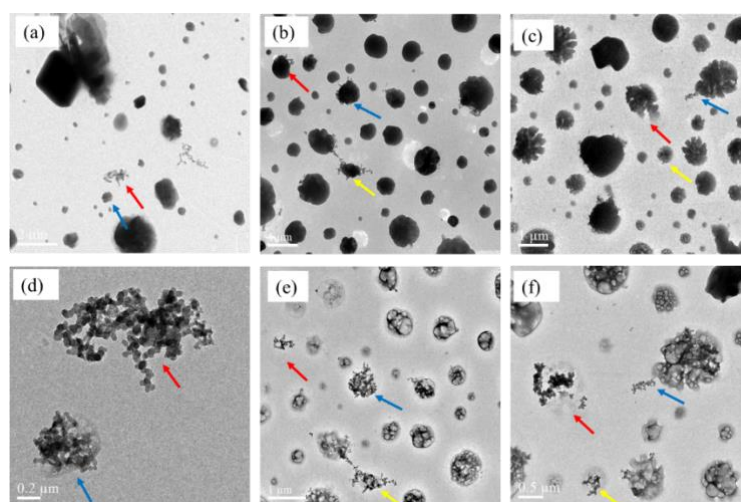
---

## 5. TEM images and EDS spectrum of the BC particles and the tar balls

Figure S6 shows the TEM images of the three Navigation samples before and after beam focus, revealing the presence of external and internal BC particles. Figure S7 presents the representative single particles and their corresponding EDS spectra for the navigation samples, indicating that the major components are: (a, c) BC and sulfate, (b) sulfate, (d) sea salt, organics and BC. Notably, detecting nitrogen (N) element in EDS is challenging due to its high vaporization rate, whereas potassium (K) serves as a tracer for biomass-burning in the BC- and sulfate-containing particles.

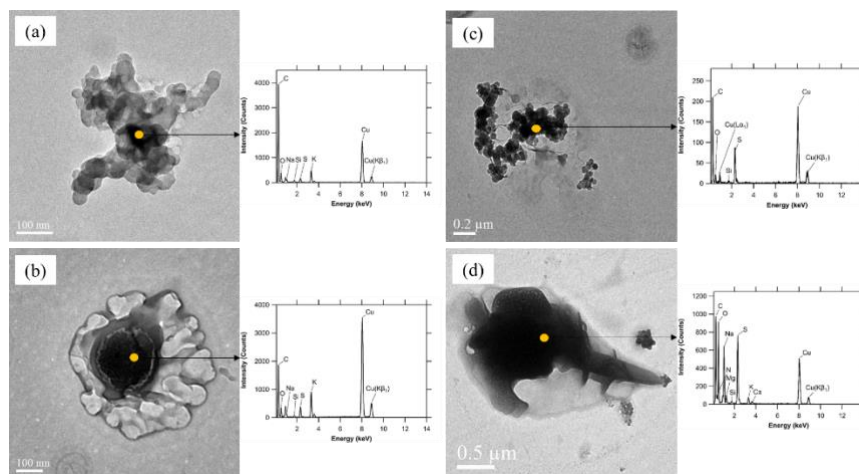
The stop samples, shown in Figure S8, exhibit both internal mixtures and externally large aggregates of the BC particles. The EDS point analysis of freshly emitted BC particles in Figure S8c reveals the presence of very thin coating elements. In summary, the stop single particles were influenced by both the own ship emissions and long-range transport air masses.

Figure S9 depicts example images of tar balls mixed with black carbon in the geometrical size range of 159–190 nm from the single particles collected during stop on May 14 and 23, 2021. The backward trajectories suggest that the air masses were originated from the Philippines, possibly due to biomass burning during those days. Figure S10 shows example images of pure BC particles, consisting of nano-soot particles with a diameter of 40–50 nm. Obviously, the size of tar balls is significantly larger than that of nano-soot spheres.

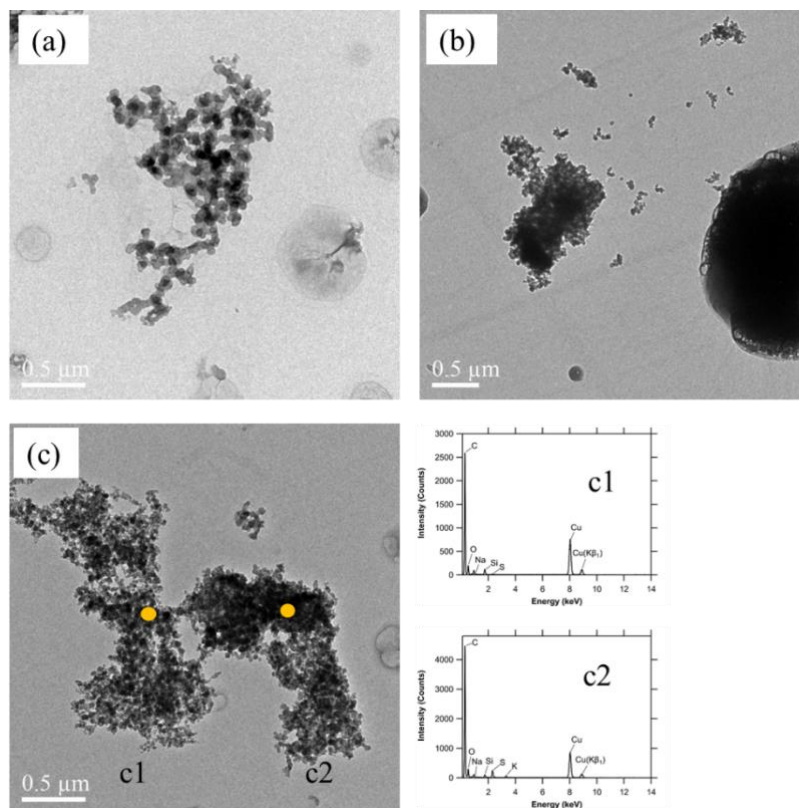


120 **Figure S6.** The example TEM images before (a, b, and c) and after (d, e and f) electron beam focus for the single particles collected during navigation. The same color arrows in each pair of images (a and d, b and e, c and f) indicate the same single particles.



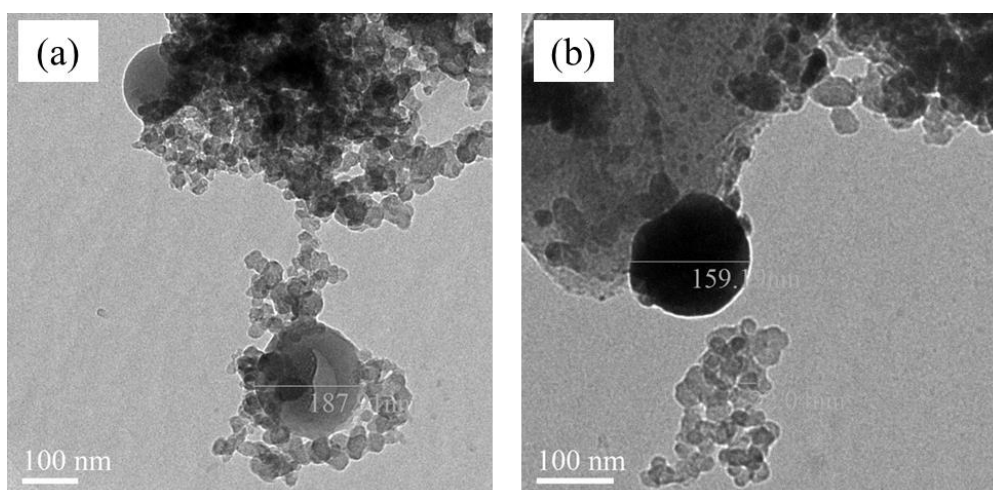


**Figure S7.** Examples of the EDS spectra for the single particles from the navigation samples. Si and Cu are excluded from the particle composition. (a) BC, and thin sulfate coating ( $\text{Na}_2\text{SO}_4$ ,  $\text{K}_2\text{SO}_4$ ), (b) sulfate ( $\text{Na}_2\text{SO}_4$ ,  $\text{K}_2\text{SO}_4$ ), (c) BC, and thick sulfate coating, and (d) BC, sea salt. The orange spots indicate the point analysis of EDS spectra. The right spectrum corresponds to each left particle. The Y-axis is the intensity (counts) and X-axis is the energy (KeV).

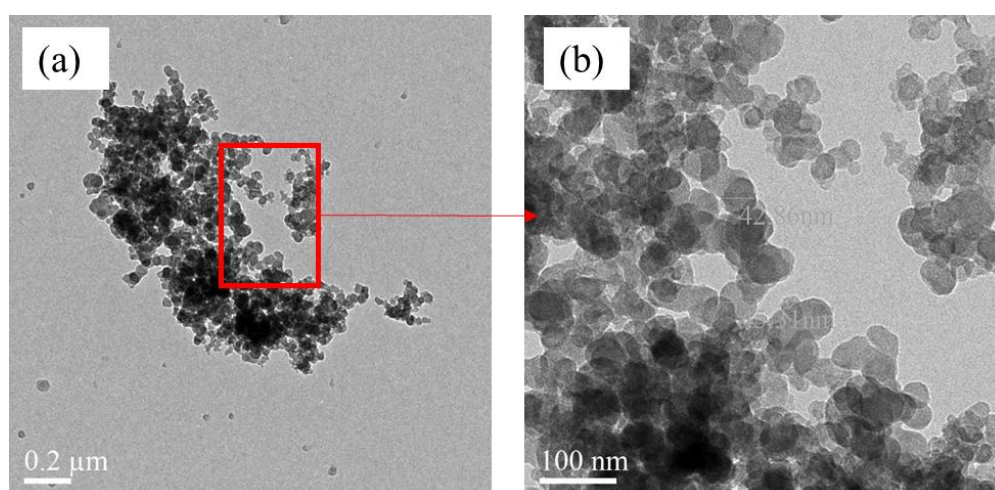


130

**Figure S8.** The example TEM images (a, b, c) of BC particles collected during stop. The orange spots indicated the point analysis of the EDS spectra (the left part c1 and the right part c2) are for the image c.



135 **Figure S9.** Example images of tar ball-containing particles collected during stop: (a) tar balls (170–190 nm) mixed with black carbon (BC) and sea salt on 10:50 May 14 2021; (b) tar balls consisted of 159 nm spherical particles on 8:39 May 23 2021.



140 **Figure S10.** Images of (a) aggregated BC particles, (b) BC made of small 40–50 nm nano-soot spheres. The S10(b) image is a magnification of the part in the red rectangle in panel a.

## 6. The diurnal average variation of OC, EC

Figure S11(a, b) shows the linear relationship between the Magee AE33 derived BC at 880 nm and the Sunset derived optical EC at 660 nm, with a time resolution of 1 min and 1h, respectively. The limit of  
 145 detection (LOD) for optical EC, as determined by the Sunset OC/EC analyzer, is  $0.062 \mu\text{g C m}^{-3}$ , based on the blank filter analysis of three times the standard deviation ( $3\sigma$ ). The fitted correlation between the

two variables in Figure S11a has a slope and intercept of the 0.97 and 0.44, respectively, with a determination coefficient ( $R^2$ ) of 0.68. However, the linear correlation between the AE33 derived BC and the Sunset EC at a time resolution of 1 h has a slope and intercept of 1.66 and -0.01, respectively, with a higher  $R^2$  of 0.91 (Figure S11b). In addition, Figure S11c displays the correlation between the optical EC and thermal EC data measured by the Sunset instrument. The slope and intercept of the fitted line are 1.55 and -0.21, respectively, with  $R^2=0.97$ . The differences of the two instruments are mainly attributed to the technical principles of the methods used for the data processing. Similar results have been reported in other studies (Brown et al., 2019).

155

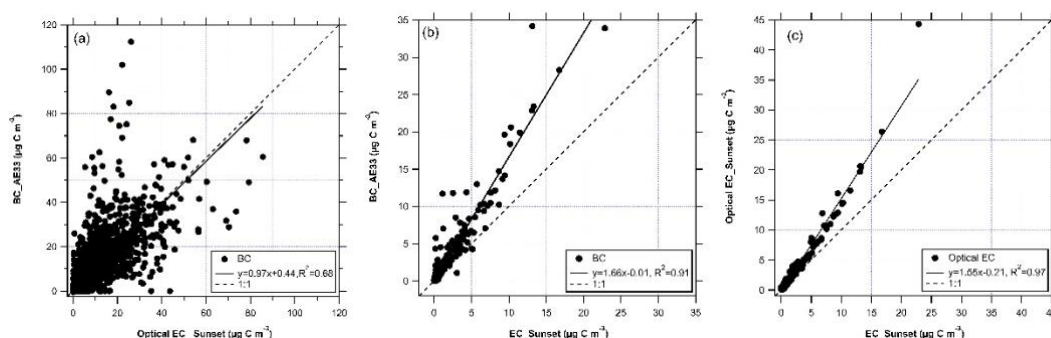
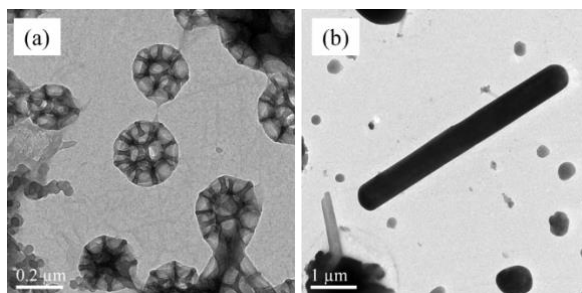


**Figure S11.** The linear relationship between the AE33 derived BC and the Sunset derived optical EC with 1-min time resolution (a), thermal EC with 1-h time resolution (b), and Sunset derived optical EC vs thermal EC with 1-h time resolution (c) for all the data during the campaign in the SCS.

## 160 7. Possible biological particles collected during the campaign

Two examples of possible biological particles were collected on two different days. Figure S12a displays brocosomes, which are known to be produced by leaf-hopping insects. This finding is supported by a previous study (Fu et al., 2012). Figure S12b depicts a rod-like particle that has yet to be identified.



165 **Figure S12.** (a) Flower-like biological particles collected at 10:50 on May 14, (b) Rod-like biological particles collected at 8:01 on May 24.

---

## 8. CALIPSO observation

Cloud-Aerosol Lidar & Infrared Satellite Observation (CALIPSO) is a remote sensor on board the TERRA and AQUA satellites. CALIPSO observation can provide vertical and horizontal distribution of the cloud and aerosol layers using the elastic backscatter intensities (extinction-to-backscatter ratio) at an Nd:YAG laser wavelength of 532 and 1064 nm near the nadir of the orbit track. CALIPSO L1 Standard V4.20 products are available from the NASA Langley Research Center ([https://www-calipso.larc.nasa.gov/tools/data\\_avail/](https://www-calipso.larc.nasa.gov/tools/data_avail/)). Images of vertical feature mask (VFM) and aerosol subtype (AS) were used to show the vertical and horizontal properties of clouds, aerosol layer and identification (Liu et al., 2019; Omar et al., 2009). Convective transport is important to the vertical distribution of aerosols (Niu et al., 2019).

Figures S13 and S14 show the orbit track location, vertical feature mask, and aerosol subtype at 6:00 on May 15, and at 19:30 on June 07, respectively. These images show that polluted continental/smoke and elevated smoke exist in the aerosol layer with an altitude of 1–3 km over the SCS regions and the Southeast Asia.

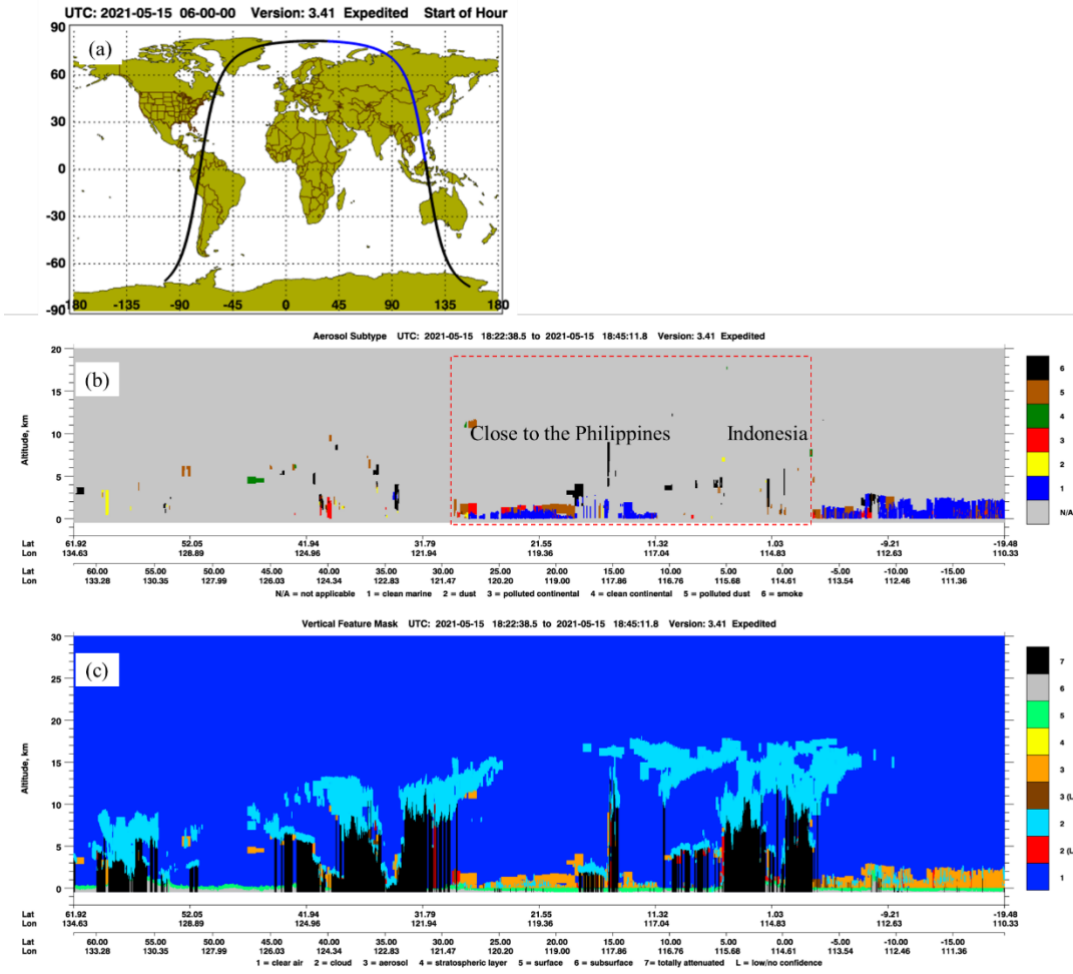
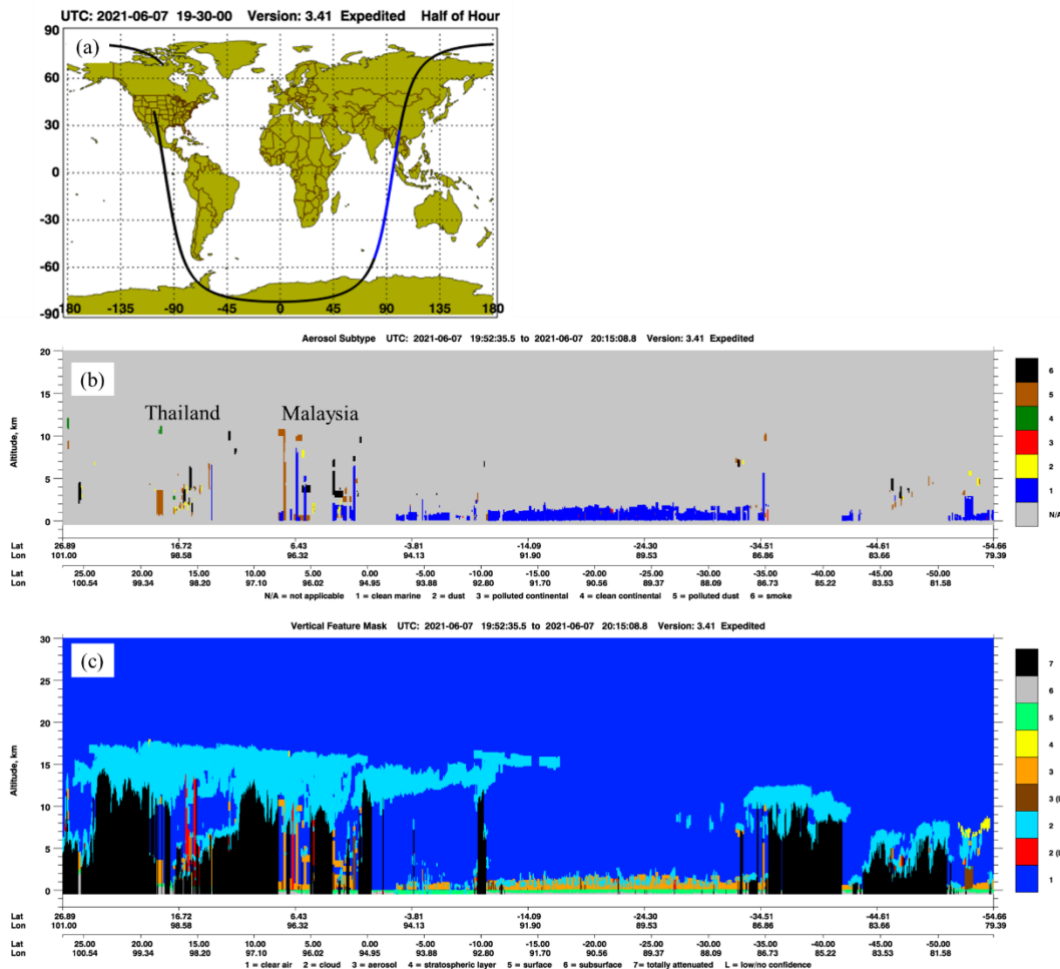


**Figure S13.** (a) Orbit track location indicated by blue curve, (b) vertical feature mask, and (c) aerosol subtype at UTC 6:00 on May 15, a time before the summer monsoon started in the SCS.



185

**Figure S14.** (a) Orbit track location indicated by blue curve, (b) vertical feature mask, and (c) aerosol subtype at UTC 19:30 on June 07, a time after summer monsoon passed in the SCS.

## References

- Brown, S., Minor, H., O'Brien, T., Hameed, Y., Feenstra, B., Kuebler, D., Wetherell, W., Day, R., Tun, R., Landis, E., and Rice, J.: Review of Sunset OC/EC instrument measurements during the EPA's Sunset carbon evaluation project, *Atmosphere (Basel)*, 10, 287, <https://doi.org/10.3390/atmos10050287>, 2019.
- Fu, H., Zhang, M., Li, W., Chen, J., Wang, L., Quan, X., and Wang, W.: Morphology, composition and mixing state of individual carbonaceous aerosol in urban Shanghai, *Atmos. Chem. Phys.*, 12, 693–707, <https://doi.org/10.5194/acp-12-693-2012>, 2012.
- Liu, Y., Zhu, Q., Wang, R., Xiao, K., and Cha, P.: Distribution, source and transport of the aerosols over Central Asia, *Atmos. Environ.*, 210, 120–131, <https://doi.org/10.1016/j.atmosenv.2019.04.052>, 2019.
- Marple, V. A. and Olson, B. A.: Sampling and measurement using inertial, gravitational, centrifugal, and thermal techniques, in: *Aerosol measurement: Principles, techniques, and applications*, edited by: Kulkarni, P., Baron, P. A., and Willeke, K., John Wiley and Sons, Hoboken, New Jersey, USA, 129–151, <https://doi.org/10.1002/9781118001684.ch8>, 2011.
- Niu, H., Kang, S., Gao, W., Wang, Y., and Paudyal, R.: Vertical distribution of the Asian tropopause aerosols detected by CALIPSO, *Environ. Pollut.*, 253, 207–220, <https://doi.org/10.1016/j.envpol.2019.06.111>, 2019.
- Omar, A. H., Winker, D. M., Vaughan, M. A., Hu, Y., Trepte, C. R., Ferrare, R. A., Lee, K.-P., Hostetler, C. A., Kittaka, C., Rogers, R. R., Kuehn, R. E., and Liu, Z.: The CALIPSO automated aerosol

- 
- classification and Lidar ratio selection algorithm, *J. Atmos. Ocean. Technol.*, 26, 1994–2014, <https://doi.org/10.1175/2009jtecha1231.1>, 2009.
- 210 Zhang, K., Allen, G., Yang, B., Chen, G., Gu, J., Schwab, J. J., Felton, D., and Rattigan, O.: Joint measurements of PM<sub>2.5</sub> and light-absorptive PM in woodsmoke-dominated ambient and plume environments, *Atmos. Chem. Phys.*, 17, 11441–11452, <https://doi.org/10.5194/acp-17-11441-2017>, 2017.